macromol

MDPI

Article

Intein-Mediated Reconstitution of Split Lumazine Synthase for Programmable Protein Nanocage Assembly

Suyeon Shin [1], Ju Hwan Kim [1] and Hansol Kim [1,2,*]

[1] Department of Nanoscience and Engineering, INJE University, Gimhae 50834, Republic of Korea
[2] Department of Innovative Pharmaceutical Sciences and Engineering, INJE University, Gimhae 50834, Republic of Korea
* Correspondence: hsk@inje.ac.kr

Abstract

Background/Objectives: Protein nanocages are versatile platforms with potential applications in drug delivery, enzyme encapsulation, and bioreactor systems, owing to their precise self-assembly and excellent biocompatibility. However, most protein cage systems have limited accessibility to their internal space, which hinders the efficient encapsulation of large molecules or complex proteins. **Methods and results:** In this study, we propose a programmable reassembly system by artificially splitting the monomer of lumazine synthase, a protein that naturally forms a nanocage through self-assembly. Using intein-mediated protein splicing, the self-assembly of the monomer was converted into a condition-dependent reaction, enabling the incorporation of large or functional biomolecules prior to the assembly stage. Furthermore, to achieve targeted delivery, an EGFR-binding affibody (EGFRAfb) was fused to the split monomer so that it is exposed on the cage surface after reassembly, thereby providing selective binding capability toward EGFR-expressing cells. Successfully reassembled nanocages were visualized, and the fluorescent proteins encapsulated within them were delivered to the target and activated in specific cells. **Conclusions:** Therefore, the programmable protein nanoplatform presented in this study can overcome the spatial limitations of conventional protein cages while allowing for precise control over both the timing of cage assembly and targeted molecular delivery.

Keywords: protein nanocage; split protein; self-assembly; trans-splicing; cargo encapsulation; targeted delivery; biosensor; bioreactor

Check for updates

Academic Editor: Bruce P. Lee

Received: 10 April 2026
Revised: 18 May 2026
Accepted: 21 May 2026
Published: 3 June 2026

Copyright: © 2026 by the authors. Licensee MDPI, Basel, Switzerland. This article is an open access article distributed under the terms and conditions of the Creative Commons Attribution (CC BY) license.

1. Introduction

Protein nanocages are precisely self-assembled architectures composed of multiple subunits, which provide structurally defined platforms [1]. These nanocages, often derived from viral capsids or metabolic enzymes, have several advantages, including uniform size and structure, biocompatibility, biodegradability, and genetic/chemical modifiability, making them attractive candidates for drug delivery, biosensing, and catalytic applications [2–5]. Their hollow architecture allows for the encapsulation of a wide range of cargo molecules such as small molecules, nucleic acids, and proteins, thereby protecting and facilitating controlled interaction with biological environments [6–9].

Lumazine synthase from *Aquifex aeolicus* (AaLS) is a thermostable protein cage derived from a hyperthermophile, consisting of 60 identical subunits and symmetric icosahedral structure with an overall diameter of ~16 nm [10–12]. AaLS nanocages have narrow pores at the three-fold (~0.7 nm) and five-fold (~0.9 nm) symmetry axes, allowing for the

diffusion of small molecules [13,14]. These structural properties, along with its high thermal stability and chemical robustness, have made AaLS a widely used platform for molecular encapsulation, multivalent display, and nanoreactor design [15–18]. AaLS nanocages are usually produced in *Escherichia coli* as fully assembled particles during recombinant expression and purification [19,20]. Although the spontaneous self-assembly of AaLS is advantageous for structural integrity, this inhibits the encapsulation of large molecules into the internal cavity. Conventional strategies for encapsulating large cargos within protein nanocages are commonly based on two approaches: transient disassembly of the cage followed by reassembly in the presence of cargo, or co-expression of the cage and cargo proteins fused to complementary interaction motifs that promote encapsulation during self-assembly [21–23]. The disassembly/reassembly approach generally needs harsh conditions such as extreme pH change, high ionic strength, or chemical denaturants, which affect cargo stability [11,24,25]. AaLS is highly thermostable, which makes it resistant to controlled disassembly under mild conditions and thus unsuitable for this strategy. Co-expression methods are difficult to control cargo loading due to different expression levels between the cage and cargo proteins and can only be applied to protein cargos.

Split protein technology is used to divide a functional protein into inactive fragments that reconstitute into the native structure under specific conditions [26,27]. This strategy has been applied to re-engineer protein nanostructures with controllable and modular assembly. For example, split GFP and luciferase have been widely utilized in biosensing, protein–protein interaction assays, and intracellular tracking [28–33]. Split inteins are distinct in that they do not serve as functional proteins themselves but instead catalyze protein trans-splicing, ligating two protein fragments into a single, continuous polypeptide chain [34–38]. This traceless site-specific ligation has been widely used to reconstitute other split proteins with high precision.

In this study, we report a novel strategy for conditionally assembling protein nanocages by rationally splitting the AaLS monomer into two fragments, each fused to complementary halves of a split intein. Unlike wild-type AaLS, these split fragments do not self-assemble during expression or purification, thereby remaining in a pre-assembly state. Upon triggering intein-mediated trans-splicing, the full-length AaLS monomer is reconstituted, which subsequently self-assembles into a functional cage structure. This approach decouples the expression/purification process from nanocage formation and allows for controlled timing of cage assembly.

The key advantage of this platform lies in its ability to encapsulate large molecules within the cage interior by simply mixing them with split monomers prior to reconstitution. This circumvents the need for harsh disassembly/reassembly cycles and enables encapsulation under mild, physiological conditions. Moreover, the strategy provides temporal control over cage formation, offering potential applications in controlled release, intracellular assembly, and stimuli-responsive delivery systems.

2. Materials and Methods

2.1. Chemicals

DL-Dithiothreitol (DTT) and ProLong™ Diamond Antifade Mountant with DAPI was purchased from Invitrogen™ (Thermo Fisher Scientific, Waltham, MA, USA). A Cell Counting Kit-8 (CCK-8) was acquired from Dojindo Laboratories (Kumamoto, Japan).

2.2. Plasmid Construction

To create the split intein-containing plasmids (pET30b-AaLS$_N$-Int^N, pET30b-AaLS$_N$-ST-Int^N, and pET30b-Int^C-AaLS$_C$-EGFRAfb), the N- and C-terminal AaLS sequences were amplified from the previously constructed pETDuet-AaLS(R108C)-antibody binding Z

domain-ST (AaLS-Z-ST) plasmid and cloned into the pET30b plasmid containing the N- or C-intein sequence. Briefly, the split AaLS sequence was amplified by PCR using primers designed for Gibson assembly. The final product of that set of genes was mixed with Gibson Assembly® Master Mix (New England Biolabs, Ipswich, MA, USA) at a ratio of 1:1 (v/v) and transformed into Escherichia coli DH5α cells. pETDuet-SC-SuperNovaRed was also produced using pETDuet-SC-SuperNovaRed-EGFRAfb in-house as a template in the same manner. The recombinant plasmids were purified in the yesP™ Plasmid Mini Kit (GenesGen, Busan, Republic of Korea) according to the manufacturer's protocol.

2.3. Purification of Proteins

The plasmids formed from AaLS were transformed into Escherichia coli BL21 (DE3) cells and grown in 1 L of Luria–Bertani (LB) medium containing 50 μg/mL kanamycin at 37 °C until the optical density at 600 nm (OD600) reached 0.6. Proteins were induced by the addition of 500 μM Isopropyl β-D-1-thiogalactopyranoside (IPTG) at 25 °C for 18–20 h. SC-SuperNovaRed protein was grown in LB medium containing 50 mg/mL ampicillin and induced with 1 mM IPTG, then cultured at 20 °C for over 20 h. The cells were harvested by centrifugation at 4500× *g* at 4 °C, and the cell pellet was resuspended in 50 mL of Lysis buffer containing 20 mM Tris-HCl, 300 mM KCl, 0.4 mM EDTA, 10 mM imidazole, 0.1% Triton X-100 and 10% glycerol at pH 7.2. To maintain stable protein structures, 0.2 mM PMSF and 1 mM DTT were added immediately prior to resuspension. The cell walls were lysed by adding lysozyme at a final concentration of 0.05 mg/mL and undergoing sonication, and cellular debris was removed by centrifugation at 13,000× *g* for 1 h at 4 °C. Proteins in the supernatant were purified with immobilized metal affinity chromatography (IMAC) with Ni Sepharose 6 fast flow resin (Cytiva, Marlborough, MA, USA). IMAC-purified proteins were concentrated using 10 kDa cut-off centrifugal filter (Amicon® Ultra centrifugal Filter, Merck-Millipore, Darmstardt, Germany) and quantified by the BCA assay (Pierce BCA Protein Assay Kit, Thermo Scientific, Waltham, MA, USA). The amino acid sequence of all protein structures in this study was provided (Figure S1).

2.4. Intein Mediated Trans-Splicing Assay

The reaction was performed by mixing N-terminal and C-terminal intein precursor proteins in pH 6.5, 7.4 and 8.0 1X PBS containing 1 mM EDTA, followed by the addition of 4 mM DTT. The ligation product of the two exteins was confirmed by SDS-PAGE analysis, and the presence of DTT and the time and ratio conditions were optimized. Splicing was performed by incubating each fragment, N- and C-terminal intein proteins, at ratios of 1:1, 1:1.5, 1:2, 1.5:1 or 2:1 with 4 mM DTT at 37 °C for 2 h. Changes in ligation were observed over various time ranges (0, 15, 30 min, 1, 2, 4, 8, 24, 48 h) in the presence of DTT, compared to the product mixed in the absence of reducing agent. The spliced monomer generated under the final conditions was verified by dynamic light scattering (DLS) analysis (Zetasizer Nano ZS90, Malvern Panalytical, UK). The DLS measurements were performed in triplicate after equilibration at 25 °C for 120 s. Number-based size distribution was used accurately to compare the protein fragments, the generated monomers, and the self-assembled cages. Protein splicing efficiency was calculated using ImageJ software (version 1.54p, National Institutes of Health, Bethesda, MD, USA).

2.5. Reassembly of Spliced Monomer

To ensure a stable protein nanocage assembly structure, the spliced monomers were dialyzed overnight in 1X PBS buffer at pH 6.5, 7.4 or 8.0 to remove residual DTT used in the splicing process. The assembled nanocages were confirmed based on whether peaks corresponding to the expected diameter and approximate value were measured via DLS analysis.

To selectively encapsulate SpyCatcher fusion proteins within the reassembled cage, $AaLS_{N\text{-}ST}$-Int^N was reacted with either SC-mEGFP or SC-SuperNovaRed. Reaction conditions were set to achieve a 1:1, 1:2, or 2:1 ratio of ST to SC proteins at 37 °C for 2 h, or at 37 °C with a 1:1 ratio for 3, 6, or 12 h. The ligation products were then verified by SDS-PAGE. A 50 kDa cut-off centrifugal filter was used to remove residual SC-fusion protein excluding the ligation product. Splicing was performed under optimized conditions by adding the C fragment and 4 mM DTT. After 24 h, the protein was dialyzed overnight in pH 6.5 1X PBS, and the cage diameter was confirmed by DLS measurement.

2.6. TEM Imaging

For TEM analysis, protein nanoparticle samples in distilled water were blotted on carbon TEM grids (CF200-Cu, Electron Microscopy Sciences, Morgantown, PA, USA), then negatively stained using 2% uranyl acetate. Images were obtained using transmission electron microscope (JEM-2100; TEMCON software, JEOL Ltd., Tokyo, Japan).

2.7. Cell Culture

The breast cancer cell line MCF7, which expresses a small amount of EGFR, was purchased from the American Type Culture Collection (ATCC, Manassas, VA, USA), and the over-expressing cell line MDA-MB-468 was obtained from the Korean Cell Line Bank (KCLB, SNU, Seoul, Republic of Korea). Both cell lines were cultured in Dulbecco's Modified Eagle Medium (DMEM; Biowest, Nuaillé, France) medium containing 1% (v/v) antibiotic-antimycotic (Gibco, Thermo Fisher Scientific, Waltham, MA, USA) and 10% fetal bovine serum (FBS; Biowest), maintained at 37 °C in a 5% CO_2 environment.

2.8. Flow-Cytometry

For flow cytometry to confirm target delivery, MCF7 and MDA-MB-468 cells at a density of 1×10^5 were transferred into sterile microtubes. To remove residual 0.25% Trypsin–EDTA (Gibco, Thermo Fisher Scientific, Waltham, MA, USA), cells were resuspended in 1 mL BD Pharmingen™ Stain Buffer (FBS) (BD Biosciences, San Jose, CA, USA) and centrifuged three times at 1500× g for 5 min. The supernatant was discarded, and the cell pellet was resuspended in 500 µL of fresh buffer. The protein diluted in 1X PBS to a final concentration of 1 µM was then mixed for 1 h at 4 °C. Reassembled cages encapsulating mEGFP were measured for fluorescence on the FITC channel, while reassembled cages encapsulating SuperNovaRed were measured in the TexasRed channel. Flow cytometry was performed using a NovoCyte Advanteon system (Agilent Technologies, Santa Clara, CA, USA).

2.9. Cell Viability and PDT Assay

All cytotoxic assays, including photo dynamic therapy (PDT), were performed on cells seeded at a density of 1 × 104 and cultured for at least 12 h before sample treatment. In an experiment to assess simple cytotoxicity, protein samples diluted in pH 7.4 1X PBS ($AaLS_N$-Int^N, $AaLS_{N\text{-}ST}$-Int^N, Int^C-$AaLS_C$-EGFRAfb, spliced monomer, reassembled cage) were mixed with DMEM at final concentrations ranging from 20 µM to approximately 600 nM and used to treat cells for 2 h. For the phototoxic treatment effect of Reactive Oxygen Species (ROS)-forming protein (SuperNovaRed), protein samples (reassembled cage without SuperNovaRed, SC-SuperNovaRed, SC-SuperNovaRed-EGFRAfb, reassembled cage with SuperNovaRed) were diluted to a final concentration of 5 µM in DMEM and treated for 6 h, as previously described. After removing the samples, the wells were washed twice with Dulbecco's phosphate-buffered saline (DPBS; Gibco, Thermo Fisher Scientific, Waltham, MA, USA) and refilled with medium to induce stable cellular uptake of the proteins. The cells were then exposed to LED light for 3 h with the medium in

place. Then, cells were washed twice with DPBS and treated with Cell Counting Kit-8 reagent diluted 10-fold in DMEM, followed by incubation for 2–4 h. All cell viabilities were calculated based on the absorbance of non-treated cells measured at 450 nm.

2.10. Cell Imaging and ROS Detection

MCF7 and MDA-MB-468 cells were seeded at a density of 7×10^4 cells per well onto sterile cover glass in 12-well plates and cultured overnight in DMEM at 37 °C with 5% CO_2. To observe the targeted delivery of the reassembled cage encapsulating mEGFP, the protein sample diluted in 1X PBS was mixed with the medium to achieve a final concentration of 8 μM and applied to the cells for 1 h. After sample suction, we removed residual proteins by washing them twice with DPBS. To fix the cells and absorbed proteins, we added 4% paraformaldehyde (PFA) to submerge the cover glass surface and processed it in the dark for 15 min at room temperature. After removing the PFA, the residual solution was washed once with 1X PBS. The cover glass was taken for nuclear staining and reacted with DAPI for at least 30 min at room temperature under dark conditions.

To visualize the targeted delivery of the reassembled cage encapsulating SuperNovaRed and ROS formation by LED, cells were seeded in confocal dishes and cultured overnight at 37 °C with 5% CO_2. The previous medium was removed, and the cells were washed once with DPBS. The protein samples were then diluted in medium to a final concentration of 5 μM and added to the cells. After removing the protein processed for 6 h, we filled the medium and waited long enough for it to be internalized into the cells. The following day, cells were stained by incubating for 30 min in the dark with DCFH-DA diluted to a final concentration of 10 μM in DMEM without FBS. After removing the chemical agent using 1X PBS, the cells were exposed to LED light for 3 h with the medium filled. All cell imaging was performed using a confocal laser scanning microscope (LSM 800; Carl Zeiss, Oberkochen, Germany), and DCFH-DA was measured at the FITC wavelength.

3. Results and Discussion

3.1. Design Strategies for Programmable Protein Nanocage

A strategy to control the self-assembly of protein nanocages involves splitting the AaLS monomer into two fragments to temporarily restrict its self-assembly capability (Figure 1). Each fragment does not form a cage during protein purification and stably maintains its structure, while regaining proper self-assembly function upon reconstitution as a monomer. This is a simple and innovative strategy enabling internal cargo loading without artificially introducing charges or involving harsh degradation or reassembly processes. We selected the split site for the AaLS monomer based on previously reported split protein systems, such as GFP and nanoluciferase, which have been widely used for protein–protein interaction (PPI) detection [39–42]. The conditional ligation of the split protein relies on the Npu DnaE split intein fused to the N- and C-terminal AaLS fragments. In intein-mediated trans-splicing, the two precursor proteins spontaneously interact, enabling self-excision of the intein [34]. AaLS, having restored its original monomeric structure, undergoes self-reassembly in stable in vitro conditions. This is a condition-dependent method, enabling controlled assembly and manipulation of the protein nanocage.

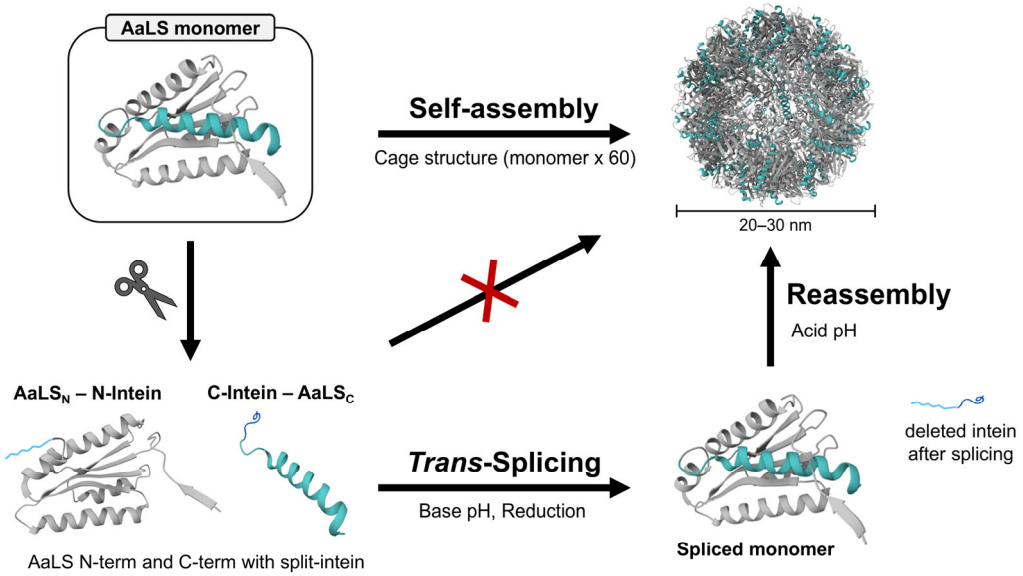


Figure 1. Schematic illustration of intein-mediated split lumazine synthase for programmable protein nanocage. To suppress the intrinsic self-assembly properties of the protein nanocage and trigger nanocage assembly under defined conditions, we propose a strategy that splits the AaLS monomer into two fragments, each containing a split intein. The two fragments do not form a cage structure during the protein purification process. Under basic pH and reducing conditions, the fragments undergo intein-mediated trans-splicing, which reconstitutes the original monomeric form and restores their ability to self-assemble.

3.2. Characterization of Split Precursor Proteins and Monomeric Structure Formation

The monomer of AaLS-wt consists of five α-helices and five β-sheets as its secondary structures. To control the self-assembly of AaLS in vitro, we selected the loop region between Thr130 and Lys131 of AaLS as the split site, because this region is structurally exposed and suitable for intein insertion without disrupting the secondary or tertiary structure after monomer reconstitution (Figure 2a). Each fragment incorporated a split intein for condition-dependent monomer reconstitution, with the N-terminal fragment (AaLS$_N$-Int^N) containing residues 1–130 of AaLS and the C-terminal fragment (Int^C-AaLS$_c$-EGFRAfb) beginning from Lys 131, the latter being fused with an EGFR-binding affibody (EGFRAfb) (Figure 2b). The N- and C-termini of the native AaLS monomer are exposed to the outer surface of the assembled cage, such that fusion of an EGFRAfb to the C-terminus of Int^C–AaLS$_c$ results in surface display of the targeting ligand after reassembly [10,43]. The designed AaLS$_N$-Int^N (27.8 kDa) and Int^C-AaLS$_C$-EGFRAfb (16.2 kDa) were purified with high purity at positions similar to their calculated standard molecular weights relative to the protein marker (Figure 2c). Two precursor proteins undergo spontaneous trans-splicing, leaving a total of six amino acids in the N-terminal intein (AEY) and the C-terminal intein (CFN) (Figure 2d) [44,45]. We used AlphaFold to predict the three-dimensional structure of the reconstituted AaLS monomer containing the residual AEYCFN amino acids at the split junction and compared the predicted structure with that of wild-type AaLS. As a result, we confirmed that despite the presence of the intein pieces, the structural similarity with wild-type AaLS was very high, with an RMSD of 0.725Å (Figure S2a,b). Residues near the intein pieces are also predicted to exhibit high similarity at 1.610 Å, indicating that insertion of the residual AEYCFN sequence did not substantially alter the local structure around the selected loop region (Figure S2c). Subsequently, we mixed the two precursor proteins in an environment containing high pH (~8.0) and a reducing agent (DTT) to induce the splicing of the monomers. The splicing efficiency was not significantly affected by the mixing ratio of two proteins, but it increased as the reaction time lengthened in the presence of DTT

(Figure S3a–c). Therefore, two proteins at equivalent molar concentrations reacted with DTT for 24 h and under optimized conditions, the spliced monomer was confirmed to have a molecular weight of 25.99 kDa, consistent with the calculated molecular weight of the reconstituted AaLS monomer and smaller than $AaLS_N$-Int^N, due to removal of the intein (~17 kDa) (Figure 2e). A new band below the N-fragment, resulting from the mixture of $AaLS_N$-Int^N and Int^C-$AaLS_C$-EGFRAfb, was found to have a splicing efficiency of 50.89% upon quantification using Image J. This splicing efficiency is consistent with the typical range reported for Npu DnaE split intein systems. Monomer formation was also confirmed by DLS measurement, showing a size shift to 6–7 nm after splicing, distinct from the 1–1.5 nm fragments (Figure 2f). The surface charge was also measured to be around −8 mV due to the interaction between the $AaLS_N$-Int^N near −10 mV and the Int^C-$AaLS_C$-EGFRAfb around −2 mV (Figure S3d).

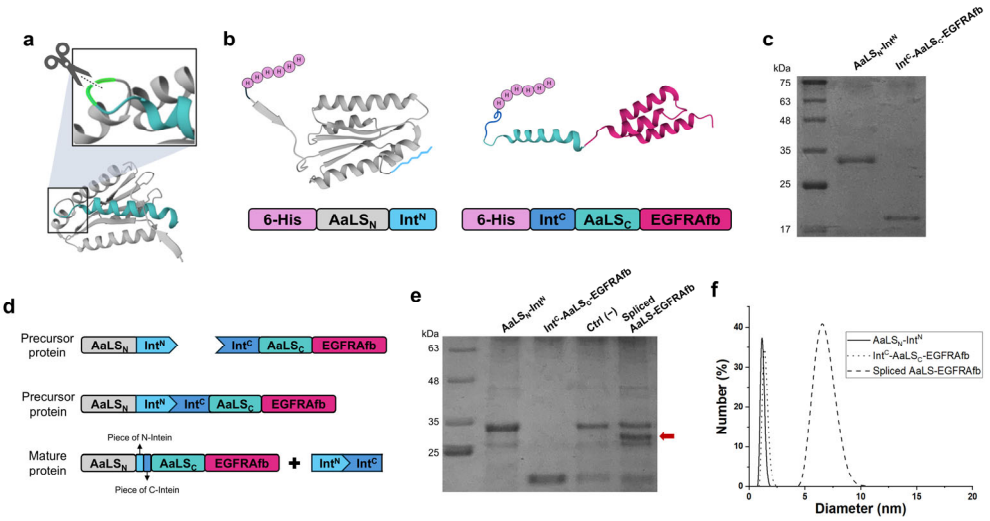
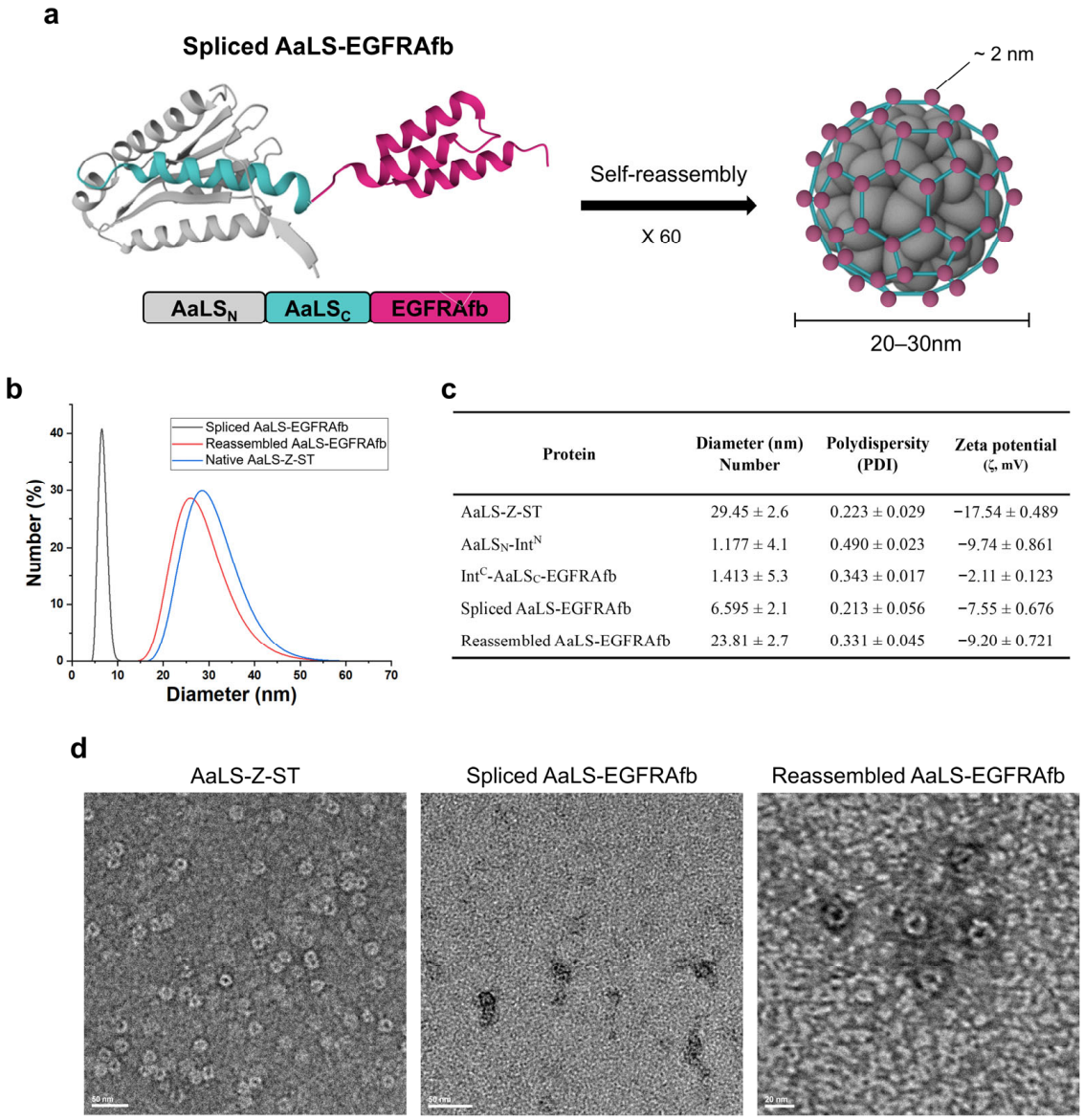


Figure 2. Design of split proteins and verification of intein-mediated trans-splicing. (**a**) AaLS-wt monomer (PDB: 5MPP) split loop region image. (**b**) Composition illustration of two split fragments. (**c**) SDS-PAGE analysis of purified $AaLS_N$-Int^N and Int^C-$AaLS_C$-EGFRAfb. (**d**) Overview of the reaction between two fragments that spontaneously form monomers through intein-mediated trans-splicing. (**e**) SDS-PAGE analysis of spliced AaLS-EGFRAfb monomer. (**f**) DLS analysis of two fragments and spliced AaLS-EGFRAfb. Molecular weight markers are indicated on the left side of the gel. Red arrow = Spliced product.

3.3. Reassembly of Protein Nanocage After Monomer Reconstitution

The intein-mediated reconstituted monomer carries an EGFR affibody fused to its C-terminus. This monomer assembles into a cage structure composed of 60 subunits, as originally designed, forming a 20–30 nm diameter nanocage with EGFRAfb displayed on the outer surface (Figure 3a). To ensure stable nanocage reassembly, we removed the DTT and lowered the pH over a sufficient period of time. DLS measurements showed that the reassembled nanocages have a diameter comparable to that of AaLS-Z-ST, with an approximate difference of 5 nm, and are clearly distinct from the monomeric species after splicing. (Figure 3b,c). The observed diameter difference between the reassembled nanocage and AaLS-Z-ST is caused by the difference in the C-terminal fusion proteins, as well as the presence of non-reassembled monomeric species that lower the average diameter. The relatively elevated PDI value of the reassembled nanocages is also considered to originate from the presence of partially assembled or non-assembled species remaining after the splicing process. Nanocage reassembly under a mildly acidic pH of 6.5, similar to the tumor microenvironment, resulted in relatively low PDI and size values close to the predicted diameter (Figure S4). The difference in nanocage formation depending on

pH is likely due to previous reports demonstrating that the arginine pairs at the subunit interface of AaLS may be responsible for the pH dependence of capsid assembly, and that at pH 7 or above, the deionization of these arginine pairs disrupts the ion network, rendering Lumazine synthase unstable [10]. For these reasons, we successfully exhibited the reassembly of the nanocages at a pH 6.5, as demonstrated by the TEM image, showing particles absent during the splicing stage but appearing after reassembly induction (Figure 3d). As a result, we engineered the self-assembly of AaLS into a condition-dependent reaction and demonstrated the potential for introducing functional proteins or macromolecules into the cage prior to reassembly.



Protein	Diameter (nm) Number	Polydispersity (PDI)	Zeta potential (ζ, mV)
AaLS-Z-ST	29.45 ± 2.6	0.223 ± 0.029	−17.54 ± 0.489
AaLS$_N$-Int^N	1.177 ± 4.1	0.490 ± 0.023	−9.74 ± 0.861
Int^C-AaLS$_C$-EGFRAfb	1.413 ± 5.3	0.343 ± 0.017	−2.11 ± 0.123
Spliced AaLS-EGFRAfb	6.595 ± 2.1	0.213 ± 0.056	−7.55 ± 0.676
Reassembled AaLS-EGFRAfb	23.81 ± 2.7	0.331 ± 0.045	−9.20 ± 0.721

Figure 3. Self-assembling capability restored in spliced monomers. (**a**) Schematic illustration of reassembly of spliced AaLS-EGFRAfb monomer. (**b**) DLS measurements of proteins after splicing, reassembly, and native AaLS-Z-ST (control). (**c**) Table data of native AaLS-Z-ST, two precursor proteins, spliced monomer, and reassembled nanocage. (**d**) TEM images of native AaLS-Z-ST, monomer after splicing, and nanocage after reassembly. Data are presented as mean ± standard deviation (SD) (n = 3). Scale bar = 50 nm in AaLS-Z-ST and Spliced AaLS-EGFRAfb, 20 nm in Reassembled AaLS-EGFRAfb.

3.4. Selective Cargo Encapsulation and Utilization of Reassembled Nanocages as Biosensors

After confirming the conditional reassembly of split AaLS, we propose a nanocage strategy that enables selective cargo encapsulation through a modular system. We fused SpyTag (ST) to the loop region of the N-terminal precursor protein to induce spontaneous ligation with the SpyCatcher (SC)-fused protein. When the ST/SC conjugated protein reassembled into a cage via intein-mediated trans-splicing with the C-terminal precursor protein, we designed a new N-terminal precursor protein with a directionally controlled SpyTag to position the SC-fusion fluorescent protein inside the cage (Figure 4a). To demonstrate the potential of reassembled nanocages as biosensors, we designed and purified the $AaLS_N$-ST-Int^N fusion protein and first confirmed its splicing pattern compared to the existing N-terminal precursor protein ($AaLS_N$-Int^N) (Figure S5a). When this protein was spliced with Int^C-$AaLS_C$-EGFRAfb to form a monomer, the predicted structure showed a very high similarity of 0.774 Å to the previously known AaLS-wt monomer (Figure S5b). We also experimentally verified that the splicing efficiency was similar under various conditions such as pH, ratio, and time (Figure S5c–e). A total of four proteins, including the completed new N-terminal precursor protein and the spliced monomer, maintained a high cell viability exceeding 70% even at high concentrations up to 20 μM, confirming the absence of significant cytotoxicity (Figure S6).

We designed and purified an SC-mEGFP (monomeric enhanced green fluorescent protein) to implement a biosensor nanocage targeting EGFR overexpressed in cells (Figure S7a). Considering that the outer diameter of the formed cage is at least 20 nm, but the inner diameter is narrower, we set an ST/SC ligation efficiency of around 10% as the optimal criterion and adjusted the ratio of the two proteins accordingly. This ligation ratio was intentionally controlled to minimize steric hindrance within the confined internal cavity of the nanocage, since excessive cargo conjugation across all subunits could interfere with stable cage assembly and structural integrity. The covalently linked product of SC-mEGFP (42.5 kDa) and $AaLS_N$-ST-Int^N (29.5 kDa) corresponds to approximately 70 kDa and exhibited a conjugation efficiency ranging from a maximum of 13.1% to a minimum of 12.7% without regulating the ratio of the two proteins (Figure S7b). Although the amount of ligation product increased with time in the ST/SC reaction, the difference was less than 2% (Figure S7c). Therefore, based on the ligation efficiency of approximately 10% already achieved for the assembly of 60 subunits into a cage, we mixed the two proteins at a molar ratio of 1:1 and reacted them for 3 h. Subsequently, unbound free SC-protein was removed, and splicing was induced. Some samples were spliced while retaining SC-mEGFP, while others were spliced without it; SC-mEGFP was completely removed (Figure 4b). We found that $AaLS_N$-ST-Int^N of a size removable by the filter in this process were not removed, unlike the larger SC-mEGFP. Subsequently, to verify whether the same pattern persisted with the same filter, we added another SC protein (SC-SuperNovaRed) containing both proteins, and more than 90% of the SC proteins were removed (Figure S8). The samples after splicing and reassembly maintained uniform diameters of 7–8 nm and 23–24 nm, respectively, as observed in DLS, similarly to previous results (Figure 4c). The EGFR targeting ability of the nanocage encapsulating mEGFP was examined by showing a localized GFP signal only near the cell membrane of cell lines overexpressing the receptor (MDA-MB-468) under identical conditions (Figure 4d). Furthermore, in EGFR-low-expressing cell lines (MCF-7), our nanocage platform (AaLS(mEGFP)-EGFRAfb) showed a negligible receptor affinity of about 2.7% compared to non-treated cells, while in overexpressing cell lines, it showed a significant GFP-positive population of 76.8% (Figure 4e). This suggests that the nanocages, which undergo a spontaneously stable reassembly phase with mEGFP, were delivered to target cells via the exposed affibody on their surface, rather than through non-specific conjugation of the protein.

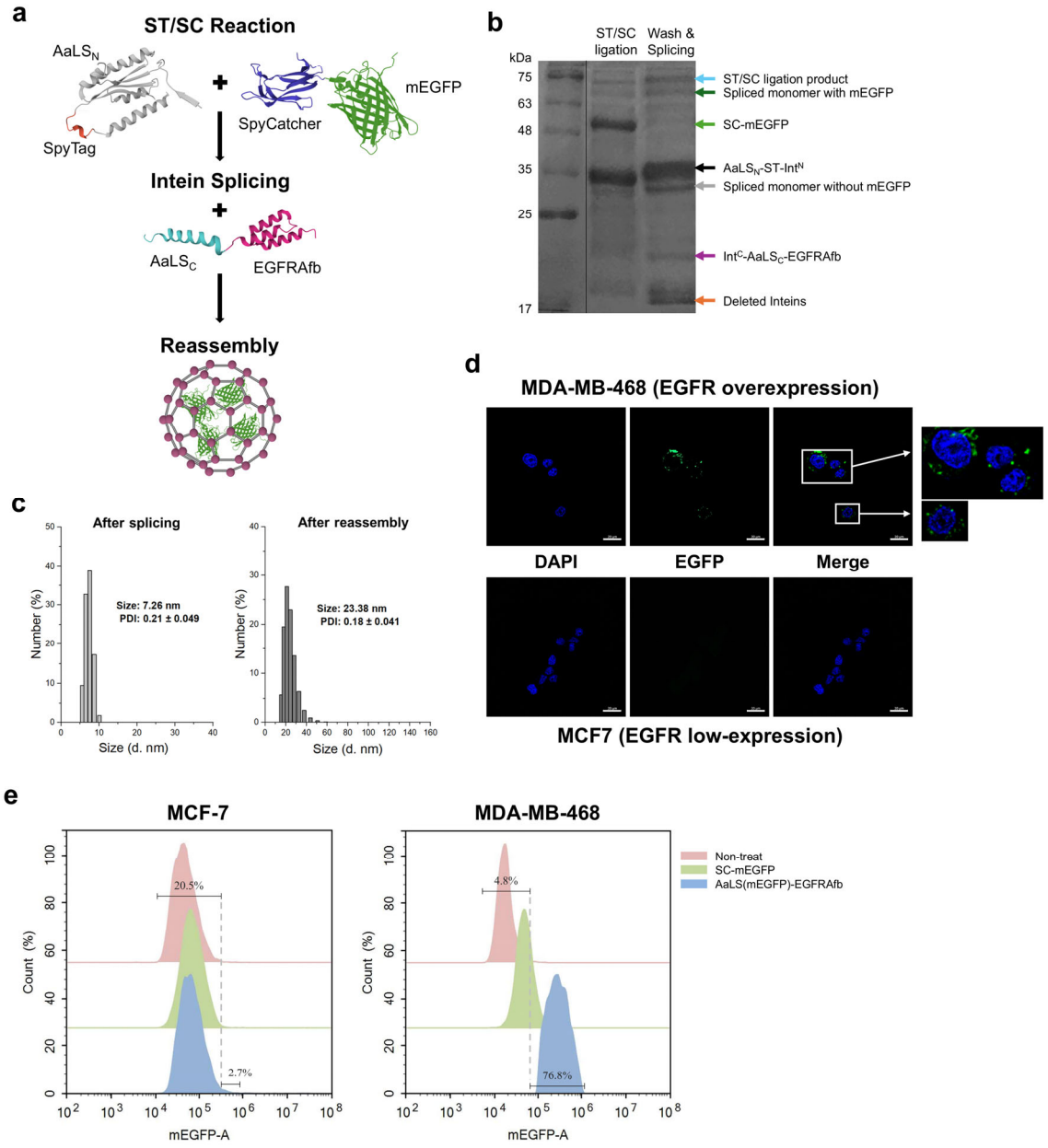


Figure 4. A reassemblable nanocage that can selectively encapsulate polymers using a modular system. (**a**) Schematic illustration shows that the N-fragment, designed with the SpyTag exposed inside the cage structure, allows the SpyCatcher to capture the fused protein within the reassembled nanocage. (**b**) SDS-PAGE analysis of proteins after removing free SC-mEGFP following ST/SC ligation and proceeding with splicing. The spliced gel segments are indicated by black lines, and all segments originate from the same original image. (**c**) DLS measurements of AaLS with mEGFP after splicing or reassembly. (**d**) Confocal images of EGFR-overexpressing MDA-MB-468 cells and low-expressing MCF-7 cells treated with reassembled AaLS(GFP)-EGFRAfb. (**e**) Flow cytometric histogram showing the difference in targeting of the nanocage platform based on EGFR expression levels in cells. Scale bar = 20 μm.

3.5. ROS-Generating Phototoxic Proteins Encapsulated in Reassembled Nanocages: As a Bioreactor

SuperNovaRed is a monomeric variant of KillerRed, a photosensitizer and fluorescent protein that generates reactive oxygen species (ROS) [46]. Compared to KillerRed, which has low utility as a fusion protein due to its tendency to form dimers, SuperNovaRed not only possesses ROS-forming capability but also exists as a monomer, making it advantageous for fusion protein application. Both proteins exhibit potent cell death effects

when exposed to green light above 500 nm and can be utilized in photodynamic therapy (PDT) [47]. After verifying the potential for selective cargo encapsulation and cage assembly, we designed a novel SC-fusion protein (SC-SuperNovaRed) to broaden the application range of this nanocage platform. When SuperNovaRed is encapsulated within the reassembled nanocages, it will function as a bioreactor that continuously generates ROS upon exposure to light in the LED wavelength range of 550 nm or higher, thereby inducing cell death (Figure 5a). SC-SuperNovaRed was purified as a monomer with a size of approximately 41 kDa (Figure S9a). When performing ST/SC ligation with $AaLS_N$-ST-Int^N, it exhibited a binding efficiency in the 10% range, similarly to previous results (Figure S9b). No significant correlation between reaction time and ligation efficiency was observed (Figure S9c). To prevent cell death caused by free SC-SuperNovaRed not encapsulated within the reassembled nanocage, these were clearly removed (Figure 5b). Subsequently, through sequential splicing and reassembly processes, a nanocage with an external diameter of approximately 22.5 nm was formed (Figure 5c). The nanocage, AaLS(SuperNovaRed)-EGFRAfb, was treated identically with a control protein lacking targeting ability in both EGFR-low-expressing and EGFR-overexpressing cell lines. In MCF-7 cells, the nanocage platform showed a negligible 0.4% increase in fluorescence compared to untreated cells, while in MDA-MB-468 cells, it exhibited a substantial 39.5% increase in fluorescence signal. The control protein SC-SuperNovaRed showed almost complete overlap with the background signal in non-treated cells, proving that this was not non-specific binding. Consequently, this suggests that the reassembled nanocage encapsulating SuperNovaRed is delivered in a manner dependent on EGFR presented on the cell membrane (Figure S10a).

The targetable nanocage platform is internalized into cells via receptor-mediated endocytosis and can activate the ROS generation capacity of SuperNovaRed within the cage through LED irradiation. To evaluate the targeting ability of this nanocage and the LED-based ROS formation of the internal enzyme protein, we evaluated its cell death capacity using a non-targeted negative control (SC-SuperNovaRed). In cells maintained in the dark, those treated with free SC-SuperNovaRed (SC-SNR) and the nanocage AaLS(SNR)-EGFRAfb retained high cell viability of 95.8% and 94.1%, respectively. However, after exposure to LED light (79–81 J/cm^2), these rates decreased to 83.25% and 55.3%. The nanocage reassembled without SuperNovaRed (AaLS-EGFRAfb) still maintained a high cell viability of 97.7%, supporting that the nanocage itself is not cytotoxic (Figure 5d). Under identical conditions, the negative cell line MCF-7 actually showed an increased cell viability of 117.1% upon LED exposure (Figure S10b). To directly observe the activity of the encapsulated enzyme proteins, EGFR-overexpressing cells were stained using DCFH-DA, which detects reactive oxygen species. As a result, SC-SNR, used as a negative control, did not internalize into target cells during the same treatment period, yielding no detectable signal (Figure 5e left). However, our nanocage platform demonstrated target delivery capability, as evidenced by a red fluorescent signal located around the cells when not exposed to LED illumination (Figure 5e right, LED(–)). Furthermore, after LED exposure, the ROS-generating ability of the delivered SuperNovaRed was activated, resulting in extensive green fluorescence observed throughout the cells (Figure 5e right, LED(+)). Additionally, we engineered SC-SuperNovaRed-EGFRAfb as a definitive positive control protein to re-evaluate the targeted delivery of the nanocage platform and ROS generation within cells. Both groups demonstrated significant cytotoxicity only when exposed to LED in EGFR-overexpressing cell lines, suggesting their inherent toxicity is negligible given the high cell viability observed without LED irradiation. Furthermore, our nanocage platform displayed a cell viability of 47.7%, while the control group (SC-SNR-EGFRAfb) showed 61.2%. This result suggests the possibility of ROS generation or increased half-life of the

enzyme protein confined within the protein cage (Figure S10c). Flow cytometry analysis further confirmed differences in ROS formation in DCFH-DA-stained MDA-MB-468 cells, with FITC fluorescence increasing by 84.4% in the positive control group and 88.8% in the nanocage-treated group relative to the non-treated group. In contrast, the non-targeted negative control showed only a minimal increase in fluorescence around 4.2% (Figure S10d). The mean fluorescence intensity of DCFH-DA was also quantified, and we demonstrated the utility of the protein nanocage as a bioreactor (Figure S10e). To determine the LED irradiation time required for cytotoxicity, we modulated the irradiation time and analyzed ROS generation by confocal microscopy. SuperNovaRed encapsulated within the nanocage platform remained intracellular at all time points and exhibited the green fluorescence intensity of DCFH-DA, generated by LED exposure time. The fluorescence observed after 4 and 8 h of LED exposure was nearly identical, indicating that ROS formation within the cells reached a saturated state by 4 h (Figure S11).

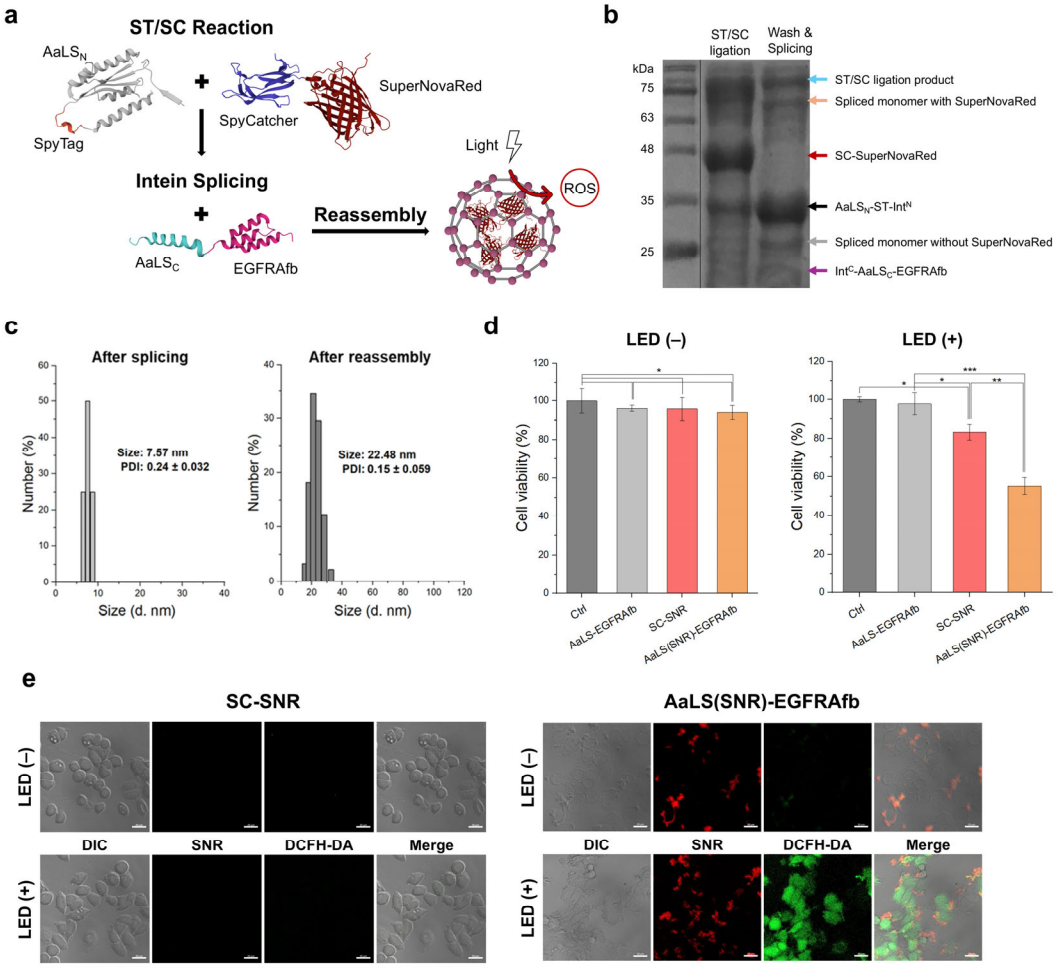


Figure 5. Photodynamic Therapy (PDT) using ROS-forming enzyme-encapsulated reassembled nanocages. (**a**) Schematic illustration of a modular reassemblable nanocage encapsulating SC-fusion SuperNovaRed to enable continuous ROS generation by LEDs within the platform. (**b**) SDS-PAGE analysis of proteins after removing free SC-SuperNovaRed following ST/SC ligation and proceeding with splicing. The spliced gel segments are indicated by black lines, and all segments originate from the same original image. (**c**) DLS measurements of AaLS with SuperNovaRed after splicing and reassembly. (**d**) Cell viability of EGFR-overexpressing cell line treated with AaLS(SNR)-EGFRAfb under LED non-irradiation versus irradiation. (**e**) Confocal microscopy images of ROS detection in EGFR-overexpressing cells treated with the SC-SNR or AaLS(SNR)-EGFRAfb platform and exposed to LED light. Scale bar = 20 μm. Statistical significance is indicated as $p < 0.05$ (*), $p < 0.01$ (**), and $p < 0.001$ (***).

Moreover, proteins encapsulated within protein nanocages are protected from environmental substances and therefore exhibit enhanced intracellular stability compared to free proteins. To evaluate the protective effect of protein nanocages on encapsulated proteins, we measured fluorescence quenching of fluorescent proteins. The quenching of fluorescent proteins typically occurs in the presence of ionic surfactants (detergents), which can also interfere with fluorescence measurements. Therefore, we used Triton X-100, a nonionic surfactant capable of inducing mild quenching without interfering with fluorescence detection. First, Triton X-100 diluted in PBS (ranging from a maximum of 1% to a minimum of 0.016%) was mixed with free SC-SuperNovaRed protein, and fluorescence intensity was measured at three time points (0.5, 1, and 1.5 h). Even with the same concentration of detergents, 0.5 h was not sufficient to quench the fluorescent protein, while 1% Triton X-100 exhibited a quenching efficiency of nearly 65% (Figure S12a). To prevent the quenching of the fluorescent protein encapsulated inside the protein nanocage, the cage structure must not collapse due to the detergent. Therefore, we mixed protein nanocages that had been reassembled without an internal protein with 1% Triton X-100 and measured the particle diameter. The results showed particle sizes of 20–30 nm, with an increase of approximately 5 nm when mixed with the detergent. This may be due to protein adsorption by the nonionic surfactant (Figure S12b). Protein nanocages encapsulating SuperNovaRed or mEGFP and free fluorescent proteins (SC-SuperNovaRed, SC-mEGFP) exhibited different fluorescence intensity patterns when reacting with detergent under the same conditions. As expected, the fluorescent proteins encapsulated within the protein nanocages exhibited a quenching rate of less than 10%, whereas the free fluorescent proteins were quenched by nearly 60% even after a short reaction timer of 30 min (Figure S12c,d). In addition, we sought to further verify the structural stability of this nanocage platform in an in vitro environment that mimics the in vivo environment. The cell culture medium contained 10% (v/v) fetal bovine serum, which provides nutrients and proteins similar to those found in an in vivo environment. Therefore, we mixed the fluorescent protein-encapsulated nanocage protein with DMEM medium containing 10% FBS (Fetal bovine serum) in a 1:1 volume ratio and cultured the mixture at 37 °C. After 6 h, we measured the fluorescence intensity of the proteins and found that the nanocage-encapsulated SuperNovaRed maintained a high fluorescence intensity of 94.4%. The nanocage-encapsulated mEGFP also retained 88.8% of its fluorescence, confirming the physical stability of the reassembled nanocage structure (Figure S12e).

4. Conclusions

To overcome the limitation of conventional protein cages in retaining large cargo molecules, we proposed a strategy for developing conditionally self-assembling protein nanocages through intein-mediated reconstitution of split AaLS. The split monomer restored the self-assembly properties of the original protein nanocage and enabled encapsulation of cargo molecules prior to cage formation. Furthermore, $AaLS_N$-ST-Int^N was designed with SpyTag exposed toward the inner cavity, enabling selective binding to SpyCatcher-fusion proteins while maintaining structural stability.

The reassembled nanocage specifically recognized EGFR-overexpressing tumor cells via a surface-displayed EGFR affibody. We experimentally demonstrated EGFR-dependent targeting using fluorescent protein cargo and further demonstrated the utility of the platform as a biosensor. Encapsulation of ROS-generating proteins also enabled LED-induced ROS generation and cytotoxicity in target cells, supporting the applicability of the reassembled nanocage as a ROS-generating bioreactor for photodynamic therapy. In addition, the nanocage protected encapsulated proteins from detergent-induced fluorescence quenching, suggesting improved cargo stability. These findings demonstrate the feasibil-

ity of a programmable protein nanocage platform for targeted delivery and functional protein encapsulation.

Supplementary Materials: The following supporting information can be downloaded at https://www.mdpi.com/article/10.3390/macromol6020039/s1, Figure S1: Amino acid sequence of proteins. The sequence of each protein is presented in the specified color, while the linker region is shown in black.; Figure S2: Structural comparison between spliced monomers and AaLS-wild type monomer. (a) Structure of the post-splicing monomer containing the intein pieces predicted by AlphaFold. (b) Comparison of structural similarity between the predicted structure and the AaLS-wt (PDB: 5MPP) monomer. (c) Structural effects of intein pieces remaining between monomer sequences after splicing. RMSD was calculated using Chimera X software. Orange = Intein pieces after splicing, Blue = AaLS-wt, Gray = spliced AaLS; Figure S3: Optimization of intein-mediated trans-splicing. (a) SDS-PAGE analysis comparing splicing reactions after mixing N-fragments (AaLSN-IntN) and C-fragments (IntC-AaLSC-EGFRAfb) at three ratio conditions (1:1, 1:2, 2:1) with 4mM DTT for 1-h. (b) Comparison of splicing efficiency based on DTT presence/absence and reaction time after mixing N-fragments and C-fragments at a 1:1 ratio. All splicing reactions were performed at 37 °C. The protein standard marker is present on the left side of the gel. Gray arrow = AaLSN-IntN, Purple arrow = Spliced monomer, Light blue arrow = IntC-AaLSC-EGFRAfb. (c) Calculated splicing efficiency depending on SDS-PAGE by Image J. (d) Surface charge differences between fragments and spliced proteins. Data are presented as mean ± standard deviation (SD) (n = 3); Figure S4: DLS measurements of reassembled spliced monomers under various pH conditions. Protein that had completed splicing reactions were dialyzed at three selected points within the pH range from slightly acid pH, mimicking the tumor microenvironment (TME), to physiological conditions, and their size and PDI were measured; Figure S5: Structural analysis of proteins designed for cargo selective encapsulation and comparative analysis of intein-mediate trans-splicing. (a) SDS-PAGE analysis of purified AaLSN-ST-IntN and IntC-AaLSC-EGFRAfb proteins. (b) Comparison of structural similarity between the predicted post-splicing protein by AlphaFold and AaLS-wt (PDB: 5MPP). The predicted structure includes the intein pieces and SpyTag and exhibits a structure highly similar to the existing monomer. RMSD was calculated using Chimera X software. Orange = Intein pieces after splicing, Green = SpyTag, Blue = AaLS-wt, Gray = spliced AaLS. (c) Comparison of splicing reactions for N-fragments containing SpyTag and C-fragments by pH, (d) ratios, and (e) times. Black arrow = AaLSN-ST-IntN, Purple arrow = Spliced monomer, Light blue = IntC-AaLSC-EGFRAfb; Figure S6: Cytotoxicity of proteins in EGFR-positive and -negative breast cancer cell lines. Each protein exhibits no EGFR expression-dependent cytotoxicity and maintains high cell viability even at high concentrations. Data are presented as mean ± standard deviation (SD) (n = 3); Figure S7: Optimization of protein nanocage formation as a biosensor. (a) SDS-PAGE analysis of SC-mEGFP protein. (b) Comparative analysis of fusion efficiency at various ratios of AaLSN-ST-IntN and SC-mEGFP. (c) Comparison of reaction time optimization and conjugation efficiency of AaLSN-ST-IntN and SC-mEGFP at a 1:1 ratio. Green arrow = SC-mEGFP, Black arrow = AaLSN-ST-IntN, White line = ST/SC ligated protein; Figure S8: Removal of SC-fusion proteins. The SC-mEGFP and SC-SuperNovaRed (SNR) that remained unbound to AaLSN-ST-IntN were removed as flow-through (more than 90%) using a 50 kDa cut-off centrifugal filter. The AaLSN-ST-IntN protein, which is smaller in size than the SC-fusion proteins, was not removed by the same filter and remained in the sample, as confirmed by SDS-PAGE analysis; Figure S9: Optimization of protein nanocage formation as a bioreactor. (a) SDS-PAGE analysis of purified SC-SuperNovaRed protein. (b) Comparative analysis of fusion efficiency at various ratios of AaLSN-ST-IntN and SC-SuperNovaRed. (c) Comparison of reaction time optimization and conjugation efficiency of AaLSN-ST-IntN and SC-SuperNovaRed at a 1:1 ratio. Red arrow = SC-SuperNovaRed, Black arrow = AaLSN-ST-IntN, White line = ST/SC ligated protein. Ligation efficiency was analyzed using Image J; Figure S10: EGFR-specific delivery of protein nanocages encapsulating SuperNovaRed and the generation of reactive oxygen species (ROS) by LED. (a) Flow cytometry histograms of the SC-SuperNovaRed and SuperNovaRed-encapsulated protein nanocage platforms in EGFR-low (MCF-7) and EGFR-overexpressing (MDA-MB-468) cell lines. (b) LED-induced cell death in MCF-7 and (c) MDA-MB-468 cells caused by a protein nanocage

reassembled without SC-SuperNovaRed (SC-SNR), SC-SNR (negative control protein) or SC-SNR-EGFRAfb (positive control protein), and a protein nanocage platform encapsulating SNR. (d) Flow cytometry histogram of ROS formation in a targeted protein nanocage platform. (e) Quantitative analysis of ROS generated by LED exposure in MDA-MB-468 cells. Data are presented as mean ± standard deviation (SD) (n = 3). Statistical significance is indicated as $p < 0.05$ (*), $p < 0.01$ (**), and $p < 0.001$ (***); Figure S11: ROS formation in an LED exposure-time-dependent SuperNovaRed-encapsulated protein nanocage platform. The reassembled protein nanocage platform encapsulating SuperNovaRed (SNR) was delivered via receptor-mediated endocytosis by targeting EGFR overexpressed on the cell surface, and ROS formation was analyzed using fluorescence imaging at 0.5, 1, 2, 4, and 8 hours after exposure to LED light. The MDA-MB-468 cell line was used, and DCFH-DA was detected on the FITC channel. Scale bar = 20 μm; Figure S12: Protein nanocage that stably encapsulates cargo molecules protects the molecules inside from detergents. (a) Quenching curves showing the reaction of Triton X-100 and 10 μM SC-SuperNovaRed at various dilutions ranging from 1% to 0.016% over time (0.5, 1.0, 1.5 h). (b) DLS measurement of the diameter of SuperNovaRed-encapsulated protein nanocage in 1% Triton X-100 or 1X PBS at 1 h. (c-d) Difference in fluorescence intensity between protein nanocages encapsulating fluorescent proteins and free fluorescent proteins in 1% Triton X-100. (e) Observation of fluorescence quenching of fluorescent proteins (SuperNovaRed and mEGFP) inside nanocages in DMEM containing 10% FBS, which mimics an in vivo environment. Data are presented as mean ± standard deviation (SD) (n = 3).

Author Contributions: Conceptualization, H.K.; methodology, S.S.; validation, S.S. and J.H.K.; formal analysis, S.S.; investigation, S.S.; resources, H.K.; data curation, S.S.; writing—original draft preparation, S.S.; writing—review and editing, H.K. and J.H.K.; visualization, S.S.; supervision, H.K.; project administration, H.K.; funding acquisition, H.K. All authors have read and agreed to the published version of the manuscript.

Funding: This work was supported by the National Research Foundation of Korea (NRF) grant funded by the Korean government (MSIT) (grant number: RS-2025-16066102) and the Bio & Medical Technology Development Program of the National Research Foundation (NRF) funded by the Ministry of Science & ICT (grant number: RS-2026-25524613).

Institutional Review Board Statement: Not applicable.

Informed Consent Statement: Not applicable.

Data Availability Statement: The data presented in this study are available upon reasonable request from the corresponding author.

Acknowledgments: The authors thank Sebyung Kang (Ulsan National Institute of Science and Technology, UNIST) for assistance with TEM imaging. During the preparation of this manuscript, the authors used ChatGPT (OpenAI, GPT-5.5) for language editing. The authors have reviewed and edited the output and take full responsibility for the content of this publication.

Conflicts of Interest: The authors declare no conflicts of interest.

Abbreviations

The following abbreviations are used in this manuscript:

EGFRAfb	Epidermal Growth Factor Receptor Affibody
AaLS	*Aquifex aeolicus* Lumazine Synthase
AaLS-Z-ST	*Aquifex aeolicus* Lumazine Synthase-Z domain-SpyTag
ST	SpyTag
SC	SpyCatcher
mEGFP	Monomeric Enhanced Green Fluorescent Protein
SNR	SuperNovaRed
ROS	Reactive Oxygen Species
PDT	Photodynamic Therapy

References

1. Edwardson, T.G.W.; Levasseur, M.D.; Tetter, S.; Steinauer, A.; Hori, M.; Hilvert, D. Protein Cages: From Fundamentals to Advanced Applications. *Chem. Rev.* **2022**, *122*, 9145–9197. [CrossRef]
2. Molino, N.M.; Wang, S.W. Caged protein nanoparticles for drug delivery. *Curr. Opin. Biotechnol.* **2014**, *28*, 75–82. [CrossRef]
3. Mallik, B.B.; Stanislaw, J.; Alawathurage, T.M.; Khmelinskaia, A. De Novo Design of Polyhedral Protein Assemblies: Before and After the AI Revolution. *Chembiochem* **2023**, *24*, e202300117. [CrossRef] [PubMed]
4. Bhaskar, S.; Lim, S. Engineering protein nanocages as carriers for biomedical applications. *NPG Asia Mater.* **2017**, *9*, e371. [CrossRef]
5. Choi, B.; Kim, H.; Choi, H.; Kang, S. Protein Cage Nanoparticles as Delivery Nanoplatforms. *Adv. Exp. Med. Biol.* **2018**, *1064*, 27–43. [CrossRef]
6. Lee, Y.; Kim, M.; Kang, J.Y.; Jung, Y. Protein Cages Engineered for Interaction-Driven Selective Encapsulation of Biomolecules. *ACS Appl. Mater. Interfaces* **2022**, *14*, 35357–35365. [CrossRef]
7. Edwardson, T.G.W.; Tetter, S.; Hilvert, D. Two-tier supramolecular encapsulation of small molecules in a protein cage. *Nat. Commun.* **2020**, *11*, 5410. [CrossRef]
8. McNeale, D.; Dashti, N.; Cheah, L.C.; Sainsbury, F. Protein cargo encapsulation by virus-like particles: Strategies and applications. *Wiley Interdiscip. Rev. Nanomed. Nanobiotechnol.* **2023**, *15*, e1869. [CrossRef] [PubMed]
9. Kwon, S.; Giessen, T.W. Engineered Protein Nanocages for Concurrent RNA and Protein Packaging In Vivo. *ACS Synth. Biol.* **2022**, *11*, 3504–3515. [CrossRef]
10. Zhang, X.; Meining, W.; Fischer, M.; Bacher, A.; Ladenstein, R. X-ray structure analysis and crystallographic refinement of lumazine synthase from the hyperthermophile *Aquifex aeolicus* at 1.6 A resolution: Determinants of thermostability revealed from structural comparisons. *J. Mol. Biol.* **2001**, *306*, 1099–1114. [CrossRef] [PubMed]
11. Seebeck, F.P.; Woycechowsky, K.J.; Zhuang, W.; Rabe, J.P.; Hilvert, D. A simple tagging system for protein encapsulation. *J. Am. Chem. Soc.* **2006**, *128*, 4516–4517. [CrossRef]
12. Wörsdörfer, B.; Woycechowsky, K.J.; Hilvert, D. Directed evolution of a protein container. *Science* **2011**, *331*, 589–592. [CrossRef]
13. Sasaki, E.; Böhringer, D.; van de Waterbeemd, M.; Leibundgut, M.; Zschoche, R.; Heck, A.J.; Ban, N.; Hilvert, D. Structure and assembly of scalable porous protein cages. *Nat. Commun.* **2017**, *8*, 14663. [CrossRef]
14. Koziej, L.; Fatehi, F.; Aleksejczuk, M.; Byrne, M.J.; Heddle, J.G.; Twarock, R.; Azuma, Y. Dynamic Assembly of Pentamer-Based Protein Nanotubes. *ACS Nano* **2025**, *19*, 8786–8798. [CrossRef]
15. Giessen, T.W.; Silver, P.A. A Catalytic Nanoreactor Based on in Vivo Encapsulation of Multiple Enzymes in an Engineered Protein Nanocompartment. *Chembiochem* **2016**, *17*, 1931–1935. [CrossRef]
16. Ren, H.; Zhu, S.; Zheng, G. Nanoreactor Design Based on Self-Assembling Protein Nanocages. *Int. J. Mol. Sci.* **2019**, *20*, 592. [CrossRef]
17. Jun, H.; Jang, E.; Kim, H.; Yeo, M.; Park, S.G.; Lee, J.; Shin, K.J.; Chae, Y.C.; Kang, S.; Kim, E. TRAIL & EGFR affibody dual-display on a protein nanoparticle synergistically suppresses tumor growth. *J. Control. Release* **2022**, *349*, 367–378. [CrossRef] [PubMed]
18. Azuma, Y.; Edwardson, T.G.W.; Terasaka, N.; Hilvert, D. Modular Protein Cages for Size-Selective RNA Packaging in Vivo. *J. Am. Chem. Soc.* **2018**, *140*, 566–569. [CrossRef]
19. Gawin, A.; Pankowski, J.; Zarechyntsava, M.; Kwasna, D.; Kloska, D.; Koziej, L.; Glatt, S.; Kachamakova-Trojanowska, N.; Azuma, Y. Encapsidic production and isolation of degradation-prone polypeptides. *J. Mater. Chem. B* **2025**, *13*, 12605–12613. [CrossRef] [PubMed]
20. Azuma, Y.; Zschoche, R.; Hilvert, D. The C-terminal peptide of *Aquifex aeolicus* riboflavin synthase directs encapsulation of native and foreign guests by a cage-forming lumazine synthase. *J. Biol. Chem.* **2017**, *292*, 10321–10327. [CrossRef] [PubMed]
21. Van de Steen, A.; Wilkinson, H.C.; Dalby, P.A.; Frank, S. Encapsulation of Transketolase into In Vitro-Assembled Protein Nanocompartments Improves Thermal Stability. *ACS Appl. Bio Mater.* **2024**, *7*, 3660–3674. [CrossRef]
22. Choi, H.; Eom, S.; Kim, H.U.; Bae, Y.; Jung, H.S.; Kang, S. Load and Display: Engineering Encapsulin as a Modular Nanoplatform for Protein-Cargo Encapsulation and Protein-Ligand Decoration Using Split Intein and SpyTag/SpyCatcher. *Biomacromolecules* **2021**, *22*, 3028–3039. [CrossRef]
23. Künzle, M.; Mangler, J.; Lach, M.; Beck, T. Peptide-directed encapsulation of inorganic nanoparticles into protein containers. *Nanoscale* **2018**, *10*, 22917–22926. [CrossRef]
24. Hori, M.; Steinauer, A.; Tetter, S.; Hälg, J.; Manz, E.M.; Hilvert, D. Stimulus-responsive assembly of nonviral nucleocapsids. *Nat. Commun.* **2024**, *15*, 3576. [CrossRef]
25. Boyton, I.; Goodchild, S.C.; Diaz, D.; Elbourne, A.; Collins-Praino, L.E.; Care, A. Characterizing the Dynamic Disassembly/Reassembly Mechanisms of Encapsulin Protein Nanocages. *ACS Omega* **2022**, *7*, 823–836. [CrossRef] [PubMed]
26. Dolberg, T.B.; Meger, A.T.; Boucher, J.D.; Corcoran, W.K.; Schauer, E.E.; Prybutok, A.N.; Raman, S.; Leonard, J.N. Computation-guided optimization of split protein systems. *Nat. Chem. Biol.* **2021**, *17*, 531–539. [CrossRef] [PubMed]

27. Bae, J.; Kim, J.; Choi, J.; Lee, H.; Koh, M. Split Proteins and Reassembly Modules for Biological Applications. *Chembiochem* **2024**, *25*, e202400123. [CrossRef] [PubMed]
28. Zhou, G.; Wan, W.W.; Wang, W. Modular Peroxidase-Based Reporters for Detecting Protease Activity and Protein Interactions with Temporal Gating. *J. Am. Chem. Soc.* **2022**, *144*, 22933–22940. [CrossRef]
29. Makhija, S.; Brown, D.; Rudlaff, R.M.; Doh, J.K.; Bourke, S.; Wang, Y.; Zhou, S.; Cheloor-Kovilakam, R.; Huang, B. Versatile Labeling and Detection of Endogenous Proteins Using Tag-Assisted Split Enzyme Complementation. *ACS Chem. Biol.* **2021**, *16*, 671–681. [CrossRef]
30. Fischer, A.A.M.; Schatz, L.; Baaske, J.; Römer, W.; Weber, W.; Thuenauer, R. Real-time monitoring of cell surface protein arrival with split luciferases. *Traffic* **2023**, *24*, 453–462. [CrossRef]
31. Romei, M.G.; Boxer, S.G. Split Green Fluorescent Proteins: Scope, Limitations, and Outlook. *Annu. Rev. Biophys.* **2019**, *48*, 19–44. [CrossRef]
32. Ishikawa, H.; Meng, F.; Kondo, N.; Iwamoto, A.; Matsuda, Z. Generation of a dual-functional split-reporter protein for monitoring membrane fusion using self-associating split GFP. *Protein Eng. Des. Sel.* **2012**, *25*, 813–820. [CrossRef]
33. Luker, K.E.; Smith, M.C.; Luker, G.D.; Gammon, S.T.; Piwnica-Worms, H.; Piwnica-Worms, D. Kinetics of regulated protein-protein interactions revealed with firefly luciferase complementation imaging in cells and living animals. *Proc. Natl. Acad. Sci. USA* **2004**, *101*, 12288–12293. [CrossRef]
34. Yao, Z.; Kim, J.; Geng, B.; Chen, J.; Wong, V.; Lyakisheva, A.; Snider, J.; Dimlić, M.R.; Raić, S.; Stagljar, I. A split intein and split luciferase-coupled system for detecting protein-protein interactions. *Mol. Syst. Biol.* **2025**, *21*, 107–125. [CrossRef]
35. Yao, Z.; Aboualizadeh, F.; Kroll, J.; Akula, I.; Snider, J.; Lyakisheva, A.; Tang, P.; Kotlyar, M.; Jurisica, I.; Boxem, M.; et al. Split Intein-Mediated Protein Ligation for detecting protein-protein interactions and their inhibition. *Nat. Commun.* **2020**, *11*, 2440. [CrossRef] [PubMed]
36. Wang, H.; Wang, L.; Zhong, B.; Dai, Z. Protein Splicing of Inteins: A Powerful Tool in Synthetic Biology. *Front. Bioeng. Biotechnol.* **2022**, *10*, 810180. [CrossRef] [PubMed]
37. Tasfaout, H.; Halbert, C.L.; McMillen, T.S.; Allen, J.M.; Reyes, T.R.; Flint, G.V.; Grimm, D.; Hauschka, S.D.; Regnier, M.; Chamberlain, J.S. Split intein-mediated protein trans-splicing to express large dystrophins. *Nature* **2024**, *632*, 192–200. [CrossRef] [PubMed]
38. Somiya, M.; Yanase, T. Programmable protein editing by split intein-mediated recombination. *bioRxiv* **2006**. 2026.2001.2022.700961. [CrossRef]
39. Ghosh, I.; Hamilton, A.D.; Regan, L. Antiparallel Leucine Zipper-Directed Protein Reassembly: Application to the Green Fluorescent ProteinClick to copy article link. *J. Am. Chem. Soc.* **2000**, *122*, 5658–5659. [CrossRef]
40. Hu, C.D.; Kerppola, T.K. Simultaneous visualization of multiple protein interactions in living cells using multicolor fluorescence complementation analysis. *Nat. Biotechnol.* **2003**, *21*, 539–545. [CrossRef]
41. Paulmurugan, R.; Gambhir, S.S. Monitoring protein-protein interactions using split synthetic renilla luciferase protein-fragment-assisted complementation. *Anal. Chem.* **2003**, *75*, 1584–1589. [CrossRef] [PubMed]
42. Remy, I.; Michnick, S.W. A highly sensitive protein-protein interaction assay based on Gaussia luciferase. *Nat. Methods* **2006**, *3*, 977–979. [CrossRef]
43. Ladenstein, R.; Schneider, M.; Huber, R.; Bartunik, H.D.; Wilson, K.; Schott, K.; Bacher, A. Heavy riboflavin synthase from Bacillus subtilis. Crystal structure analysis of the icosahedral beta 60 capsid at 3.3 A resolution. *J. Mol. Biol.* **1988**, *203*, 1045–1070. [CrossRef] [PubMed]
44. Iwai, H.; Züger, S.; Jin, J.; Tam, P.H. Highly efficient protein trans-splicing by a naturally split DnaE intein from Nostoc punctiforme. *FEBS Lett.* **2006**, *580*, 1853–1858. [CrossRef]
45. Stevens, A.J.; Sekar, G.; Shah, N.H.; Mostafavi, A.Z.; Cowburn, D.; Muir, T.W. A promiscuous split intein with expanded protein engineering applications. *Proc. Natl. Acad. Sci. USA* **2017**, *114*, 8538–8543. [CrossRef] [PubMed]
46. Takemoto, K.; Matsuda, T.; Sakai, N.; Fu, D.; Noda, M.; Uchiyama, S.; Kotera, I.; Arai, Y.; Horiuchi, M.; Fukui, K.; et al. SuperNova, a monomeric photosensitizing fluorescent protein for chromophore-assisted light inactivation. *Sci. Rep.* **2013**, *3*, 2629. [CrossRef]
47. Bulina, M.E.; Chudakov, D.M.; Britanova, O.V.; Yanushevich, Y.G.; Staroverov, D.B.; Chepurnykh, T.V.; Merzlyak, E.M.; Shkrob, M.A.; Lukyanov, S.; Lukyanov, K.A. A genetically encoded photosensitizer. *Nat. Biotechnol.* **2006**, *24*, 95–99. [CrossRef]

Disclaimer/Publisher's Note: The statements, opinions and data contained in all publications are solely those of the individual author(s) and contributor(s) and not of MDPI and/or the editor(s). MDPI and/or the editor(s) disclaim responsibility for any injury to people or property resulting from any ideas, methods, instructions or products referred to in the content.